Inorganic Chemistry

including bioinorganic chemistry

July 21, 2014
Volume 53, Number 14
pubs.acs.org/IC

ACS Publications
Most Trusted. Most Cited. Most Read.

www.acs.org

Inorganic Chemistry

JULY 21, 2014
VOLUME 53 ISSUE 14

INOCAJ 53(14) 7071–7798 (2014)
ISSN 0020-1669

ON THE COVER: A reaction between the inorganic tridecameric cluster Al_{13} and $In(NO_3)_3$ in solution leads to direct metal exchange of outer-shell aluminum ions for indium ions, resulting in new heterometallic clusters (e.g., Al_7In_6 pictured). The cover art is a digitally enhanced version of artwork designed by local Eugene, OR, artist Shanna Zentner (shannazentner@gmail.com). See M. K. Kamunde-Devonish, M. N. Jackson, Jr., Z. L. Mensinger, L. N. Zakharov, and D. W. Johnson, p 7101.

Communications

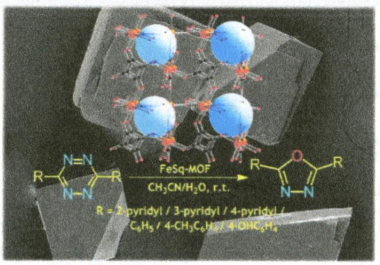

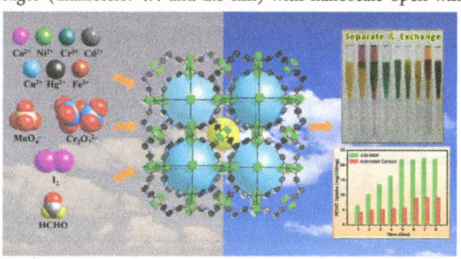

7077 (S) dx.doi.org/10.1021/ic500873y

Pyranopterin Dithiolene Distortions Relevant to Electron Transfer in Xanthine Oxidase/Dehydrogenase

Chao Dong, Jing Yang, Silke Leimkühler,* and Martin L. Kirk*

The reducing substrates 4-thiolumazine and 2,4-dithiolumazine have been used to form Mo^{IV}-product complexes in xanthine oxidase (XO) and xanthine dehydrogenase (XDH). The Mo^{IV}-product complexes absorb in the near-infrared (NIR) region of the spectrum. Optical pumping into this NIR metal-to-ligand charge-transfer band reveals in-plane bending modes of the bound product in addition to low-frequency molybdenum dithiolene and pyranopterin dithiolene (pyranopterin ditholene) vibrational modes. The work provides insight into how pyranopterin ditholene is coupled to redox changes at the Mo site and how pyranopterin ditholene functions as an electron-transfer conduit in the oxidative half-reaction of XO/XDH.

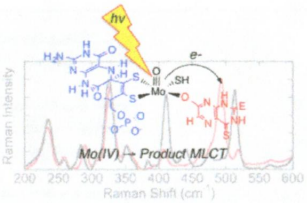

7080 (S) dx.doi.org/10.1021/ic500980j

Aza-Crown-Ether-Appended Xanthene: Selective Ratiometric Fluorescent Probe for Silver(I) Ion Based on Arene–Metal Ion Interaction

Ippei Takashima, Anna Kanegae, Manabu Sugimoto, and Akio Ojida*

A highly selective ratiometric fluorescent probe for silver(I) ion (Ag^I) has been developed based on arene–metal ion interaction. The probe showed a large-emission red shift upon binding to Ag^I. X-ray crystallography revealed that Ag^I forms a close contact with the fluorophore within the distance of the sum of their van der Waals radii. The Ag^I complex of the probe was successfully applied to the ratiometric sensing for a cyanide anion.

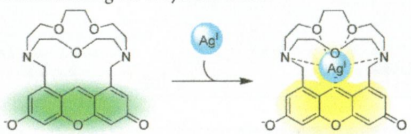

7083 (S) dx.doi.org/10.1021/ic501012e

Two Elongated Octahedral Coordination Cages Constructed by M_4-TC4A Secondary Building Units (M = Co^{II} and Fe^{II}) and 2,2′-Bipyridine-4,4′-dicarboxylic Acids

Huaqiao Tan, Shangchao Du, Yanfeng Bi, and Wuping Liao*

Two elongated octahedral coordination cages are constructed by the M_4-TC4A secondary building units and bipyridine-4,4′-dicarboxylic acid (bpdc) linkers by a [6 + 8] condensation, which have 12 apertures, 8 triangular apertures on the octahedral facets and 4 quadrilateral ones on the equatorial edges. The bpdc molecules point in different directions.

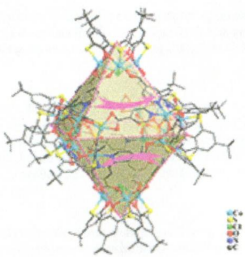

7086 dx.doi.org/10.1021/ic5012764

Porous Zirconium Metal–Organic Framework Constructed from 2D → 3D Interpenetration Based on a 3,6-Connected kgd Net

Rongming Wang,* Zhiying Wang, Yuwen Xu, Fangna Dai, Liangliang Zhang, and Daofeng Sun*

A new type of 3D interpenetrating porous zirconium metal–organic framework (**1**) based on a 2D 3,6-connected kgd net has been synthesized and characterized for the first time. The gas uptake and catalytic properties of **1** have been studied.

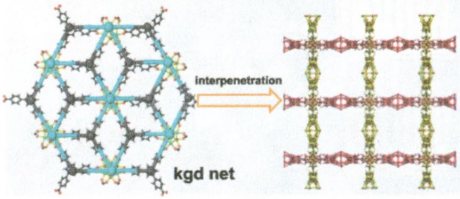

7089 dx.doi.org/10.1021/ic501341x

High-Pressure Synthesis, Crystal Structure, and Unusual Valence State of Novel Perovskite Oxide $CaCu_3Rh_4O_{12}$

Ikuya Yamada,* Mikiko Ochi, Masaichiro Mizumaki, Atsushi Hariki, Takayuki Uozumi, Ryoji Takahashi, and Tetsuo Irifune

A novel perovskite oxide, $CaCu_3Rh_4O_{12}$, has been synthesized under 15 GPa and at 1273 K. Synchrotron X-ray powder diffractiometry and Rietveld refinement indicate that this compound crystallizes in a cubic $AA'_3B_4O_{12}$-type quadruple perovskite structure. Synchrotron X-ray absorption and photoemission spectroscopy demonstrate that the valence state of this compound is $Ca^{2+}Cu^{\sim 2.8+}{}_3Rh^{\sim 3.4+}{}_4O_{12}$.

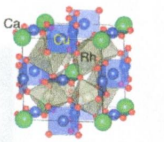

$CaCu_3B_4O_{12}$

B-site ion		
8	9	10
Fe^{4+}	$Co^{3.25+}$	Ni
Ru^{4+}	$Rh^{3.4+}$	Pd
Os	Ir^{4+}	Pt^{4+}

Articles

7092 dx.doi.org/10.1021/ic402803s

Two Three-Dimensional Lanthanide Frameworks Exhibiting Luminescence Increases upon Dehydration and Novel Water Layer Involving in Situ Decarboxylation

Ai-Hong Yang, Ji-Yong Zou, Wen-Min Wang, Xue-Ying Shi, Hong-Ling Gao, Jian-Zhong Cui,* and Bin Zhao

Two three-dimensional lanthanide coordination polymers of Tb and Yb were obtained by the hydrothermal method of in situ decarboxylation. The decarboxylation occurred under high temperature and low pH. For the Tb complex, the luminescence intensity increases when the water is driven off. When the dehydrated sample is soaked in water, the water molecules cannot be recovered. For the Yb complex, the novel two-dimensional water layer containing T8(4)10(4) water tape as the substructure is present.

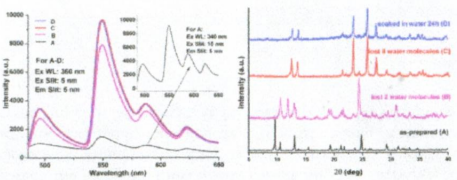

7101 S dx.doi.org/10.1021/ic403121r

Transmetalation of Aqueous Inorganic Clusters: A Useful Route to the Synthesis of Heterometallic Aluminum and Indium Hydroxo—Aquo Clusters

Maisha K. Kamunde-Devonish, Milton N. Jackson Jr., Zachary L. Mensinger, Lev N. Zakharov, and Darren W. Johnson*

A transmetalation reaction produces a new $[Al_7In_6(\mu_3\text{-}OH)_6(\mu_2\text{-}OH)_{18}(H_2O)_{24}](NO_3)_{15}$ hydroxo—aquo cluster ($\mathbf{Al_7In_6}$) from evaporation of solutions of $\mathbf{Al_{13}}$ and $In(NO_3)_3$. Several spectroscopic techniques (^{1}H NMR, ^{1}H-DOSY, DLS, and Raman) are used to compare $\mathbf{Al_7In_6}$ to its $\mathbf{Al_{13}}$ counterpart. A thin film of aluminum indium oxide (AIO) was prepared from an $\mathbf{Al_7In_6}$ cluster ink, showing its utility as a precursor for thin film materials.

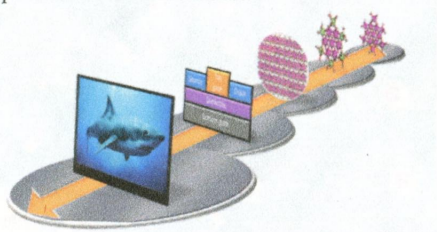

7106 S dx.doi.org/10.1021/ic4031365

Tuning the Extended Structure and Electronic Properties of Gold(I) Thienyl Pyrazolates

Lyndsey D. Earl, Jeffrey K. Nagle, and Michael O. Wolf*

The photophysical, electrochemical, and structural properties of new gold(I) cyclic trinuclear complexes depend on the conjugation length and torsion angle of the bridging thiophene-pyrazolate ligand. DFT calculations verify that the observed dual emission is ligand localized and sensitized by aurophilic interactions.

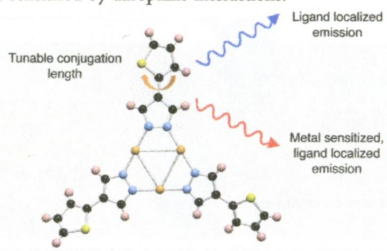

7118 S dx.doi.org/10.1021/ic403153f

Unprecedented Application of Flexible Bis(pyridyl-tetrazole) Ligands To Construct Helix/Loop Subunits To Modify Polyoxometalate Anions

Xiu-Li Wang,* Na Li, Ai-Xiang Tian, Jun Ying, Tian-Jiao Li, Xiao-Ling Lin, Jian Luan, and Yang Yang

By introducing the unprecedented and flexible isomeric bis(pyridyl-tetrazole) ligands into the Ag/POMs system, three POM-based metal—organic complexes with different Ag—bptzb subunits have been successfully obtained. The structural diversity indicates that the isomers 4- and 3-bptzb exhibit key influences on the construction of three compounds with helix/loop structures or not. Compound **3** shows excellent photocatalytic activity and selectivity for degradation of MB.

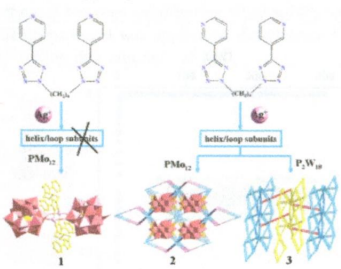

7130 dx.doi.org/10.1021/ic500008c

Probing Ligand Effects on O–O Bond Formation of Ru-Catalyzed Water Oxidation: A Computational Survey

Runhua Kang, Kejuan Chen, Jiannian Yao,* Sason Shaik, and Hui Chen*

For mononuclear Ru-based water oxidation catalysts (WOCs), our systematic DFT calculations have identified and rationalized that there are several factors affecting the O–O bond formation process: (1) a phenyl or carbene group cis to the proton-accepting moiety in the WNA mechanism; (2) the net charge of the system; and (3) steric hindrance for a very bulky ligand in the I2M mechanism. All of these factors can potentially be subjects of adjustment in future ligand design.

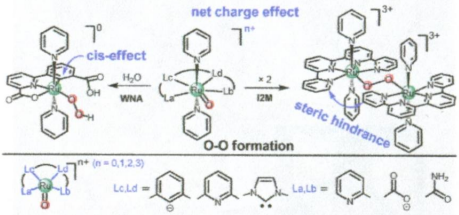

7137 dx.doi.org/10.1021/ic500121f

Electrocatalytic Proton Reduction by a Dicobalt Tetrakis-Schiff Base Macrocycle in Nonaqueous Electrolyte

Subhadeep Kal, Alexander S. Filatov, and Peter H. Dinolfo*

Dicobalt tetrakis-Schiff base type macrocycles, Co_2L^{2+} and Co_2LAc^{+}, have been synthesized, and their structural, electronic, and photophysical properties have been investigated. Electrochemical scans in the presence of trifluoroacetic acid as a H^+ source reveal electrocatalytic waves for H^+ reduction with rate constants of 138 and 63 M^{-2} s^{-1} for Co_2L^{2+} and Co_2LAc^{+} respectively. These complexes represent a new class of Co-based electrocatalytic H^+ reduction catalysts that utilize a bimetallic active site.

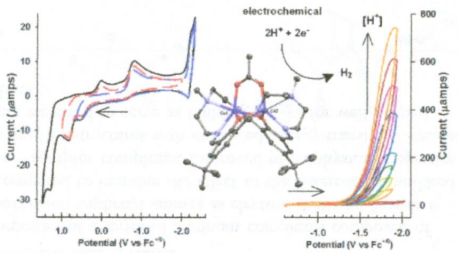

7146 dx.doi.org/10.1021/ic500128y

Solid-State NMR Structure Characterization of a ^{13}CO-Labeled Ir(I) Complex with a *P,N*-Donor Ligand Including Ultrafast MAS Methods

Andrey A. Tregubov, Rasmus Linser, Khuong Q. Vuong, Aditiya Rawal, John D. Gehman, and Barbara A. Messerle*

Solid-state NMR can provide significant information about molecular structure. Ultrafast MAS greatly improves the resolution in the ^1H dimension of 2D solid-state experiments, allowing correlations that provide valuable information about the structure of metal complexes.

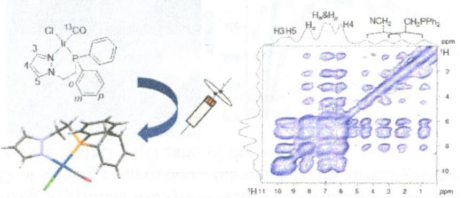

7154 dx.doi.org/10.1021/ic500181t

Expansion of the Rich Structures and Magnetic Properties of Neptunium Selenites: Soft Ferromagnetism in $Np(SeO_3)_2$

Kariem Diefenbach, Jian Lin, Justin N. Cross, Naresh S. Dalal, Michael Shatruk, and Thomas E. Albrecht-Schmitt*

The new Np^{IV} selenite, $Np(SeO_3)_2$, exhibits soft ferromagnetism.

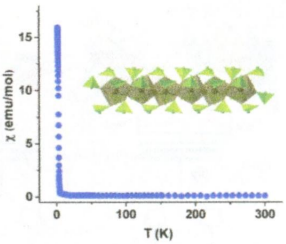

7160 dx.doi.org/10.1021/ic500213h

Stereoelectronic Effects in C–H Bond Oxidation Reactions of Ni(I) N-Heterocyclic Carbene Complexes

Rebecca C. Poulten, Isidoro López, Antoni Llobet, Mary F. Mahon, and Michael K. Whittlesey*

Exposure of three-coordinate Ni(I) N-heterocyclic carbene complexes to O_2 results in the rapid oxidation of an N-substituent C–H bond with N-Mes substituted ligands. With less bulky *ortho*-tolyl based ligands or less electron-rich amidocarbenes, very different mononuclear Ni(II) products are formed as a result of ligand redistribution.

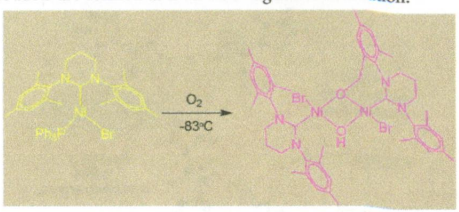

7170 dx.doi.org/10.1021/ic501196q

Ring-Shaped Rhenium(I) Multinuclear Complexes: Improved Synthesis and Photoinduced Multielectron Accumulation

Tsuyoshi Asatani, Yuki Nakagawa, Yusuke Funada, Shuhei Sawa, Hiroyuki Takeda, Tatsuki Morimoto, Kazuhide Koike, and Osamu Ishitani*

In the presence of triethanolamine, ring-shaped Re(I) tetranuclear and hexanuclear complexes can photochemically accumulate four and five electrons in a single molecule, respectively. We succeeded in much improving the synthetic yield for these complexes compared with the previously reported method.

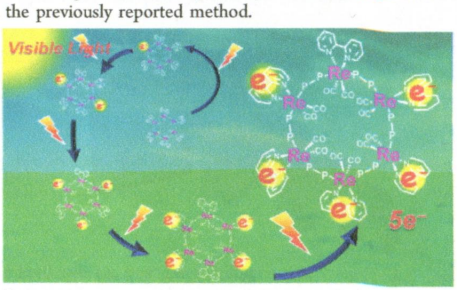

7181 dx.doi.org/10.1021/ic500266f

Luminescent Calix[4]arene-Based Metallogel Formed at Different Solvent Composition

Jaehyeon Park, Ji Ha Lee, Justyn Jaworski, Seiji Shinkai, and Jong Hwa Jung*

A calix[4]arene derivative containing terpyridine was synthesized, and it was shown that gelation occurred in the presence of Pt^{2+} in solutions of DMSO/H_2O of varying compositions. Interestingly, the metallogel showed strong luminescence enhancement, which depended on the DMSO/H_2O ratio of the solvent.

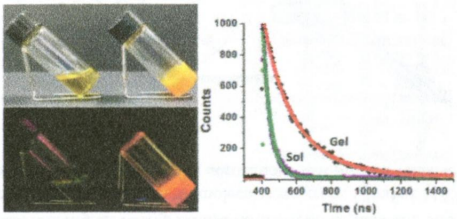

7188 dx.doi.org/10.1021/ic500290m

Synthesis and Characterization of Electron Donor–Acceptor Platinum(II) Complexes Composed of *N,N*-Diphenylpyridineamine and Triphenylamine Ligands

Zhi Dai, Alejandro J. Metta-Magaña, and Jose E. Nuñez*

The synthesis and electronic properties of a series of platinum complexes composed of triphenylamines and pyridine-derivatized triphenyl amines as electron-donating ligands is reported. Their properties are compared to examine the effect of the heteroatom-modified ligand on the properties of donor–acceptor complexes. Improved photophysical properties of the derivatives in this work may lead to structures with enhanced energy transfer. Extended derivatives of these complexes are expected to serve as building blocks for well-defined donor–acceptor metallic assemblies.

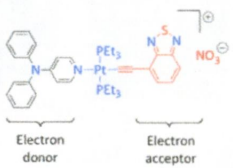

7197 dx.doi.org/10.1021/ic500295r

$^2_\infty[Bi_2Cl_6(pyz)_4]$: A 2D-Pyrazine Coordination Polymer As Soft Host Lattice for the Luminescence of the Lanthanide Ions Sm^{3+}, Eu^{3+}, Tb^{3+}, and Dy^{3+}

Johanna Heine, Tobias Wehner, Rüdiger Bertermann, Andreas Steffen, and Klaus Müller-Buschbaum*

The layered coordination polymer $^2_\infty[Bi_2Cl_6(pyz)_4]$ functions as a suitable host lattice for *in situ* co-doping of the lanthanide ions Sm^{3+}, Eu^{3+}, Tb^{3+}, and Dy^{3+} to give the luminescent networks $^2_\infty[Bi_{(2-x)}Ln_xCl_6(pyz)_4]$ with an efficient antenna effect. Emission is mainly lanthanide centered, whereas all parts of the network including bismuth can function for light uptake.

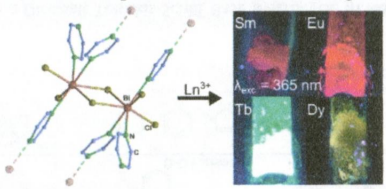

7204 S dx.doi.org/10.1021/ic500828s

Is Higher Ratio of Monoclinic to Tetragonal in $LaVO_4$ a Better Luminescence Host? Redispersion and Polymer Film Formation

Reena Okram, Ningombam Yaiphaba, Raghumani Singh Ningthoujam,* and Nongmaithem Rajmuhon Singh*

Crystalline $LaVO_4:Eu^{3+}$ nanophosphors (NPs) show the enhanced luminescence in the red region after codoping of Li^+, Sr^{2+}, and Bi^{3+} irrespective of tetragonal or monoclinic phase. Polymer film of NPs exhibits luminescence in red region. Materials will be useful in optical devices.

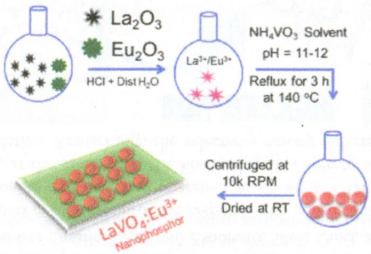

7214 S dx.doi.org/10.1021/ic5003644

Electrochemical Behavior of Phosphine-Substituted Ruthenium(II) Polypyridine Complexes with a Single Labile Ligand

Go Nakamura, Masaya Okamura, Masaki Yoshida, Takayoshi Suzuki, Hideo D. Takagi, Mio Kondo, and Shigeyuki Masaoka*

Three newly synthesized phosphine-substituted ruthenium polypyridine complexes exhibited distinct differences in their electrochemical behavior; reduction of ***cis*-PN** resulted in *cis–trans* isomerization to ***trans*-PN**, and that of **PP** proceeded via a two-electron-transfer reaction.

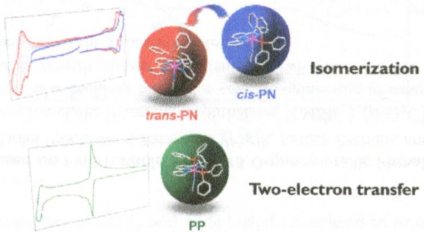

7227 S dx.doi.org/10.1021/ic5003836

Improving SERS Activity of Inositol Hexaphosphate Capped Silver Nanoparticles: Fe^{3+} as a Switcher

Xiaoyu Guo, Yichen Fu, Shuyue Fu, Hui Wang, Tianxi Yang, Ying Wen, and Haifeng Yang*

Fe^{3+} improved SERS activity of inositol hexaphosphate capped silver nanoparticles (IP_6@AgNPs) was found. The improvement mechanism of the production of more hot spots through dragging the gap between neighboring IP_6@AgNPs to ~1 nm by interaction of Fe^{3+} with IP_6 was explored. Fe^{3+}–IP_6@AgNPs-based SERS protocol was applied to detect trace thymine. The low SERS activity of the aged IP_6@AgNPs could be recovered by adding due amounts of Fe^{3+}.

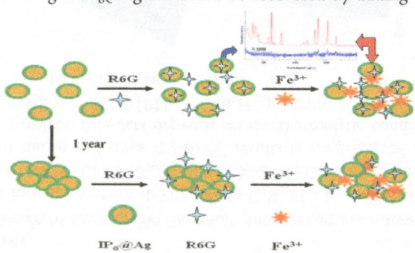

7233 dx.doi.org/10.1021/ic500390j

Titanium–Oxo Cluster with 9-Anthracenecarboxylate Antennae: A Fluorescent and Photocurrent Transfer Material

Yin-Yin Wu, Xiao-Wen Lu, Miao Qi, Hu-Chao Su, Xiao-Wei Zhao, Qin-Yu Zhu,* and Jie Dai*

9-Anthracenecarboxylate (9-AC) is selected as a photoactive ligand and two titanium–oxo clusters are prepared. The fluorescence of the cluster can be turned off by irradiating and turned on by oxygen bubbling. The photocurrent conversion property of the clusters indicates that 9-AC is an effective photosensitizer for TiO clusters.

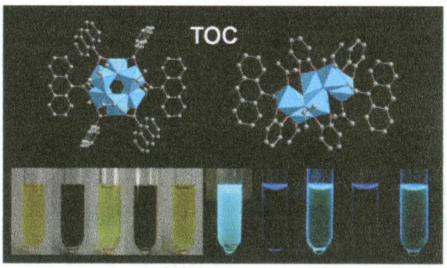

7241 dx.doi.org/10.1021/ic500470z

Borane-Protected Cyanides as Surrogates of H-Bonded Cyanides in [FeFe]-Hydrogenase Active Site Models

Brian C. Manor, Mark R. Ringenberg, and Thomas B. Rauchfuss*

A series of triarylborane adducts of $[Fe_2(dithiolate)(CO)_4(CN)_2]^{2-}$ were prepared. The FeCN-BAr_3 interaction mimics the hydrogen bonding between the protein and the active site of the [FeFe] hydrogenases. These borane adducts sustain protonation and oxidation, unlike the unprotected dicyanide complexes.

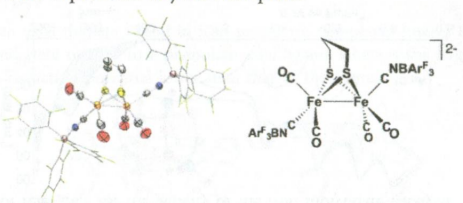

7248 dx.doi.org/10.1021/ic500549z

Coordination of a Hemilabile Pincer Ligand with an Olefinic Backbone to Mid-to-Late Transition Metals

Brittany J. Barrett and Vlad M. Iluc*

The coordination chemistry of a neutral *t*PCH=CHP pincer (*t*PCH=CHP = 2,2′-bis(di-*iso*-propylphosphino)-*trans*-stilbene) with first-row transition metals was investigated. Hemilabile behavior was observed for cobalt(II), iron(II), and copper(I) complexes.

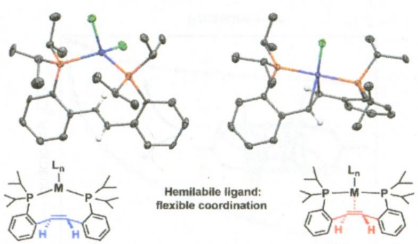

7260 dx.doi.org/10.1021/ic5005424

Luminescent Gold and Silver Complexes with the Monophosphane 1-(PPh_2)-2-Me-$C_2B_{10}H_{10}$ and Their Conversion to Gold Micro- and Superstructured Materials

Olga Crespo,* Carlos Díaz, Colm O'Dwyer, M. Concepción Gimeno,* Antonio Laguna, Isaura Ospino, and Maria Luisa Valenzuela

Gold and silver complexes with the monophosphane 1-PPh_2-2-Me-$C_2B_{10}H_{10}$ have been synthesized. Solid-state pyrolysis of [AuCl(1-PPh_2-2-Me-$C_2B_{10}H_{10}$)] and [Au_2(μ-1,12-$C_2B_{10}H_{10}$)(1-PPh_2-2-Me-$C_2B_{10}H_{10}$)$_2$] in air and of solutions of [AuCl(1-PPh_2-2-Me-$C_2B_{10}H_{10}$)] deposited on silicon and silica at 800 °C results in single-crystal Au, confirmed by diffraction and SEM-EDS. The morphology of the pyrolytic products depends on the thermolytic conditions, and different novel 3-D superstructures or microcrystals are possible. [M(7,8-(PPh_2)$_2$-$C_2B_9H_{10}$)(1-PPh_2-2-Me-$C_2B_{10}H_{10}$)] (M = Ag, Au) and [Au_2(μ-1,n-$C_2B_{10}H_{10}$)(1-PPh_2-2-Me-$C_2B_{10}H_{10}$)$_2$] (n = 2, 12) are emissive.

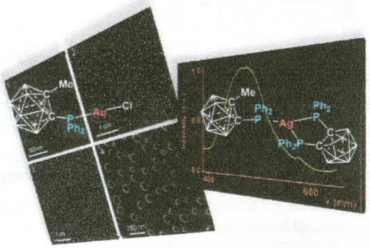

7270 S dx.doi.org/10.1021/ic5005598

Toward Coordination Polymers Based on Fine-Tunable Group 13 Organometallic Phthalates

Iwona Justyniak,* Wojciech Bury, Daniel Prochowicz, Katarzyna Wójcik, Janusz Zachara, and Janusz Lewiński*

A homologue series of group 13 organometallic macrocyclic phthalates [(MMe_2)$_2$(μ-O_2C)$_2$-1,2-C_6H_4]$_2$ (where M = Al, Ga, In) was investigated as potential molecular building blocks for crystal engineering of extended metal−organic structures. Reactions of these molecular carboxylates with various monodentate Lewis bases provide the first examples of group 13 organometallic coordination polymers based on a dicarboxylate unit.

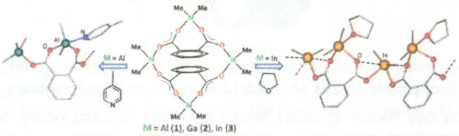

7276 S dx.doi.org/10.1021/ic500573e

Double Level Selection in a Constitutional Dynamic Library of Coordination Driven Supramolecular Polygons

Marzio Rancan,* Jacopo Tessarolo, Maurizio Casarin, Pier Luigi Zanonato, Silvio Quici, and Lidia Armelao

The introduction of tailored guests allows orchestration of the response of a constitutional dynamic library (CDL) of copper metallo-supramolecular polygons. A double level selection operates: guests act as CDL effectors driving the dynamic system toward the triangular constituent, and, at the same time, the host polygon is able to select a specific guest from a mixture according to a selectivity-affinity correlation. Remarkably, the selectivity among different guest pairs spans the $1-10^4$ range.

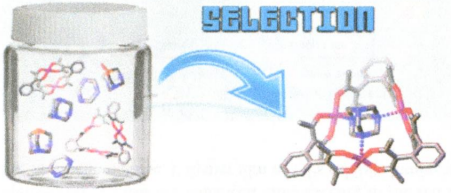

7288 dx.doi.org/10.1021/ic500629y

Robust Molecular Crystals of Titanium(IV)-oxo-Carboxylate Clusters Showing Water Stability and CO_2 Sorption Capability

Keunil Hong, Woojeong Bak, and Hyungphil Chun*

Discrete and nonporous Ti_6O_6 clusters can adsorb CO_2 depending on the carboxylate ligand.

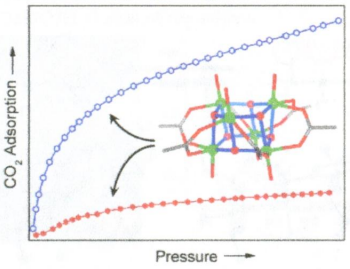

7294 dx.doi.org/10.1021/ic500584a

A Cubic Fe_4Mo_4 Oxo Framework and Its Reversible Four-Electron Redox Chemistry

Jan P. Falkenhagen, Beatrice Braun, Eckhard Bill, Dominik Sattler, and Christian Limberg*

A cubic $Fe^{II}_4Mo^{VI}_4$ oxo cluster is presented that can be oxidized successively in four single-electron processes to the all-ferric form. Three of the resulting products could be isolated, and remarkably, upon storage of the all-ferric form, one of the Mo=O corners of the cubic cage inverts, pointing toward the interior of the cage. ^{18}O/water exchanges its label with all of the oxido ligands, a finding that might be of relevance for the activity of the iron molybdate catalysts.

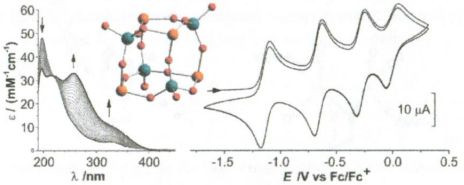

7309 dx.doi.org/10.1021/ic500630h

Preparation, Structural Characterization, and Ion-Exchange Properties of Two New Zeolite-like 3D Frameworks Constructed by ε-Keggin-Type Polyoxometalates with Binding Metal Ions, $H_{11.4}[ZnMo_{12}O_{40}Zn_2]^{1.5-}$ and $H_{7.5}[Mn_{0.2}Mo_{12}O_{40}Mn_2]^{2.1-}$

Zhenxin Zhang, Masahiro Sadakane,* Toru Murayama, Norihito Sakaguchi, and Wataru Ueda*

Two new polyoxometalate-based 3D frameworks are synthesized by connecting ε-Keggin polyoxomolybdates with different metal-ion linkers ($H_{11.4}[ZnMo_{12}O_{40}Zn_2]^{1.5-}$ and $H_{7.5}[Mn_{0.2}Mo_{12}O_{40}Mn_2]^{2.1-}$). The materials show zeolite-like ion-exchange properties.

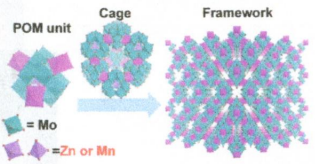

7319 Ⓢ dx.doi.org/10.1021/ic5006456

Brønsted Instead of Lewis Acidity in Functionalized MIL-101Cr MOFs for Efficient Heterogeneous (nano-MOF) Catalysis in the Condensation Reaction of Aldehydes with Alcohols

Annika Herbst, Anupam Khutia, and Christoph Janiak*

pH measurements show that the catalytic diacetalization activity of MIL-101Cr derivatives arises from Brønsted acidity of the polarized aqua ligands, which is strongly enhanced for nitro-functionalized MIL-101Cr-NO_2, giving pH values as low as 1.9. In addition, a large share of the activity is carried by small amounts of nanoscale MIL particles with diameters smaller 200 nm.

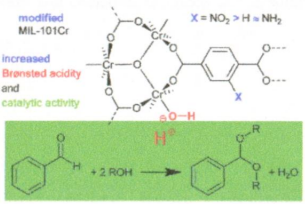

7334 Ⓢ dx.doi.org/10.1021/ic500679b

Preparation and Dehydrogenation Properties of Lithium Hydrazidobis(borane) ($LiNH(BH_3)NH_2BH_3$)

He Fu, Junzhi Yang, Xiaojuan Wang, Gongbiao Xin, Jie Zheng, and Xingguo Li*

The first example of metal-substituted hydrazine bisborane, $LiNH(BH_3)NH_2BH_3$, is synthesized and characterized by ^{11}B NMR, XRD, and FT-IR. This compound exhibits low desorption temperature (126 °C), high gravimetric hydrogen density, and satisfactory hydrogen purity, which make it a promising candidate of hydrogen storage materials.

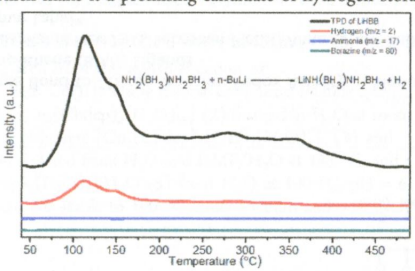

7340 dx.doi.org/10.1021/ic5006852

Excited States and Luminescent Properties of UO_2F_2 and Its Solvated Complexes in Aqueous Solution

Jing Su,* Zheming Wang,* Duoqiang Pan, and Jun Li*

As the number of coordinated water increases, the adiabatic excitation energies of $(H_2O)_nUO_2F_2$ ($n = 0–3$) are blue-shifted as a whole, and the excited states of $^3\Phi_g$ type (red) sharply go up, resulting in the dominated $^3\Phi_g$ character in all high-lying states and $^3\Delta_g$ character (black) in all low-lying excited states.

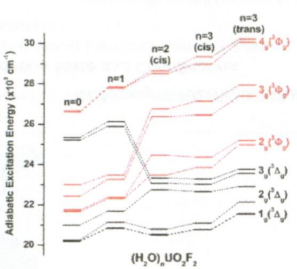

7351 S dx.doi.org/10.1021/ic5007082

Redox Potential Determines the Reaction Mechanism of HNO Donors with Mn and Fe Porphyrins: Defining the Better Traps

Lucía Álvarez, Sebastián A. Suarez, Damian E. Bikiel, Julio S. Reboucas, Ines Batinić-Haberle, Marcelo A. Martí, and Fabio Doctorovich*

The reaction mechanism and kinetics of the most widely used HNO donors Angelís Salt and toluene sulfohydroxamic acid with eight different Mn−porphyrins as trapping agents have been studied. Our results shed light into the donor decomposition mechanism and provide a thorough analysis of which MnP are the best candidates for azanone trapping and quantification experiments. The MnP redox potential determines the azanone donor reaction mechanism: oxidizing porphyrins accelerate the donor decomposition, while reducing porphyrins react with free HNO.

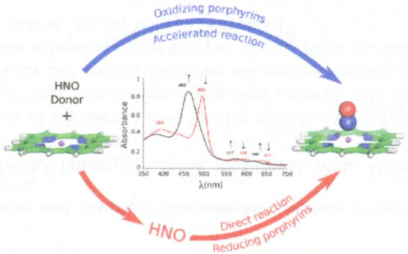

7361 S dx.doi.org/10.1021/ic500716d

Resonance Raman, Electron Paramagnetic Resonance, and Density Functional Theory Calculations of a Phenolate-Bound Iron Porphyrin Complex: Electrostatic versus Covalent Contribution to Bonding

Pradip Kumar Das and Abhishek Dey*

The large σ and π covalency of an axial thiolate ligand in iron porphyrin complexes lowers Fe−N_{pyr} bond vibration and induces a larger V/λ in the ground state relative to a phenolate axial ligand, whereas the larger electrostatic contribution to bonding in the latter results in a reduction potential lower than that of the former.

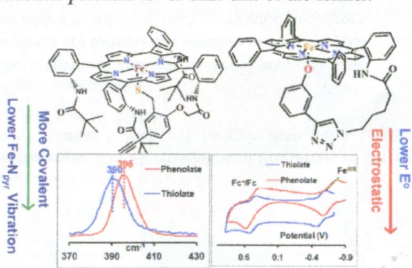

7371 dx.doi.org/10.1021/ic500718y

Redox and Luminescent Properties of Robust and Air-Stable N-Heterocyclic Carbene Group 4 Metal Complexes

Charles Romain, Sylvie Choua, Jean-Paul Collin, Martine Heinrich, Corinne Bailly, Lydia Karmazin-Brelot, Stéphane Bellemin-Laponnaz,* and Samuel Dagorne*

The coordination of a bis(aryloxide) N-heterocyclic carbene ligand to group 4 metals affords robust homoleptic complexes that are redox-active and luminesce in solution at room temperature.

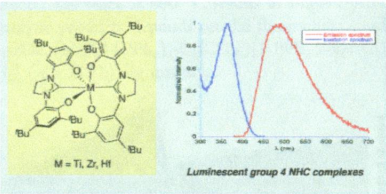

7377 dx.doi.org/10.1021/ic500728w

Chlorine-35 Solid-State NMR Spectroscopy as an Indirect Probe of Germanium Oxidation State and Coordination Environment in Germanium Chlorides

Margaret A. Hanson, Victor V. Terskikh, Kim M. Baines,* and Yining Huang

^{15}Cl solid-state NMR spectroscopy was investigated as an indirect method for the characterization of a variety of germanium chlorides. The magnitude of the C_Q [^{35}Cl] parameter was found to correlate to the assigned oxidation state of germanium and may prove useful for the assessment of the oxidation state of germanium and other main group chlorides.

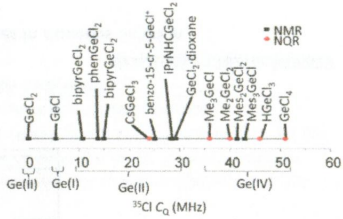

7389 dx.doi.org/10.1021/ic500730m

Sensitivity of a Strained C–C Single Bond to Charge Transfer: Redox Activity in Mononuclear and Dinuclear Ruthenium Complexes of Bis(arylimino)acenaphthene (BIAN) Ligands

Prasenjit Mondal, Hemlata Agarwala, Rahul Dev Jana, Sebastian Plebst, Anita Grupp, Fabian Ehret, Shaikh M. Mobin, Wolfgang Kaim,* and Goutam Kumar Lahiri*

π-Donating Ru^{II} effects a significant lengthening of the peri-connecting CC bond in BIAN ligands. Electron transfer to and from such compounds involves the formation of radical ligands on reduction and of Ru^{III} or Ru^{III}Ru^{II} mixed-valent species on oxidation.

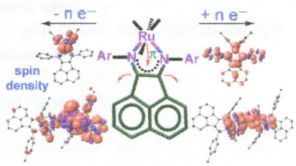

7404 dx.doi.org/10.1021/ic500757a

New Example of Hemiporphycene Formation from the Corrole Ring Expansion

Yuanyuan Fang, Federica Mandoj, Sara Nardis, Giuseppe Pomarico, Manuela Stefanelli, Daniel O. Cicero, Sara Lentini, Andrea Vecchi, Yan Cui, Lihan Zeng, Karl M. Kadish,* and Roberto Paolesse*

A new example of corrole metamorphosis, leading to a 5-hemiporphycene by regioselective ring expansion, is reported. The results obtained demonstrate that the breathing of the corrole ring can be of synthetic interest for the formation of other functionalized porphyrinoids. The coordination behavior of the obtained 5-hemiporphycene, together with detailed electrochemical characterization of the free-base and some metal complexes, shows the reactivity of the peripheral pyrazino group.

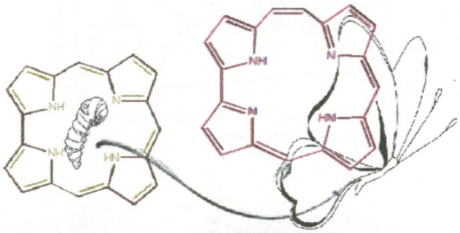

7416 dx.doi.org/10.1021/ic5007605

Effect of Axial Ligands on the Spectroscopic and Electrochemical Properties of Diruthenium Compounds

Machima Manowong, Baocheng Han,* Thomas R. McAloon, Jianguo Shao, Ilia A. Guzei, Siyabonga Ngubane, Eric Van Caemelbecke, John L. Bear, and Karl M. Kadish*

Three diruthenium complexes were synthesized with Cl, CO, or NO axial ligands and are characterized as to their electrochemical and spectroscopic properties. Different forms of diruthenium complexes are formed in a solution of $Ru_2(dpb)_4Cl$ depending on the solvent and anions added to solution. Each compound undergoes multiple redox processes involving the dimetal unit. The reversibility and potentials of the electrode reactions were found to depend on the solvent as well as the bound axial ligand.

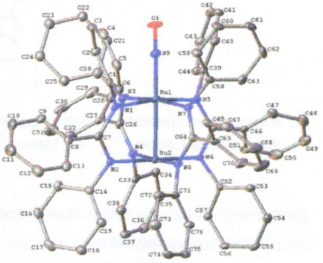

7429 dx.doi.org/10.1021/ic5007499

Synthesis, Structural Characterization, and Gas-Phase Unimolecular Reactivity of the Silver Hydride Nanocluster $[Ag_3((PPh_2)_2CH_2)_3(\mu_3\text{-}H)](BF_4)_2$

Athanasios Zavras, George N. Khairallah,* Timothy U. Connell, Jonathan M. White, Alison J. Edwards, Roger J. Mulder, Paul S. Donnelly,* and Richard A. J. O'Hair*

Mass spectrometry directed synthesis of the discrete silver hydride nanocluster $[Ag_3(\mu_3\text{-}H)(dppm)_3](BF_4)_2$, with a $[Ag_3(\mu_3\text{-}H)(dppm)_3]^{2+}$ core (see the figure), has been achieved. This nanocluster has been structurally characterized by X-ray and neutron diffraction and spectroscopically characterized to produce a well-resolved multiplet with a chemical shift at 4.5 ppm. The gas-phase dissociation chemistry has been studied and compared to that of $[Ag_3(\mu_3\text{-}H)(\mu_3\text{-}Cl)(dppm)_3]^+$.

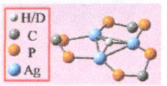

7438 dx.doi.org/10.1021/ic5007583

Synthesis of Chelating Complexes through Solid-State Dehydrochlorination Reactions via Second-Sphere-Coordination Interaction with Metal Chlorides: A Combined Experimental–Molecular Modeling Study

Hong-yu Guan, Zhen Wang, Antonino Famulari, Xu Wang, Fang Guo,* and Javier Martí-Rujas*

Combining X-ray data and DFT calculations, the mechanochemical dehydrochlorination and chelation reactions in the solid state have been monitored on a family of second-sphere complexes.

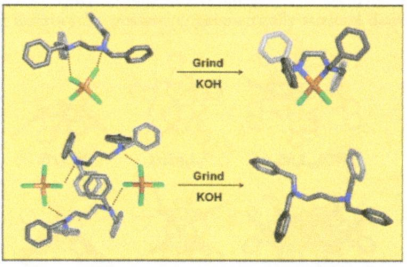

7446 dx.doi.org/10.1021/ic500789w

Transmetalation of a Dodecahedral Na_9 Aggregate-Based Polymer: A Facile Route to Water Stable Cu(II) Coordination Networks

Jin-Xiang Chen,* Ming Chen, Ni-Ni Ding, Wen-Hua Chen, Wen-Hua Zhang,* T. S. Andy Hor,* and David J. Young*

Copper-based complexes were prepared from the transmetalation of $\{Na_3[Na_9(Cbdcp)_6(H_2O)_{18}]\}_n$ (**1**) with Cu(II). These diverse complexes include a large, zwitterionic hexa-cuprometallocycle $[Cu_6(Cbdcp)_6(H_2O)_{18}]$ (**2**) formed in H_2O at room temperature, two three-dimensional polymers $[Cu_3(Cbdcp)_2(OH)_2(H_2O)_2]_n$ (**3**) and $\{[Cu_3(Cbdcp)_2(OH)_2]\cdot 2H_2O\}_n$ (**4**) isolated from H_2O and DMF/H_2O at 135 °C, and a mononuclear complex $[Cu(HCbdcp)_2(H_2O)_3]\cdot H_2O$ (**5**) from H_2O at 100 °C, pH = 6. The crystal framework of macrocycle **2** is stable to 100 °C under vacuum and selectively absorbs CO_2.

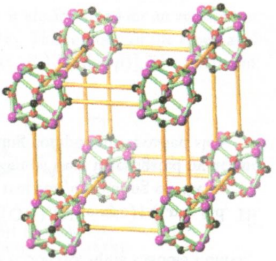

7455 dx.doi.org/10.1021/ic500771t

Straightforward Reductive Routes to Air-Stable Uranium(III) and Neptunium(III) Materials

Justin N. Cross, Eric M. Villa, Victoria R. Darling, Matthew J. Polinski, Jian Lin, Xiaoyan Tan, Naoki Kikugawa, Michael Shatruk, Ryan Baumbach, and Thomas E. Albrecht-Schmitt*

The synthesis of a family of trivalent U and Np sulfates was accomplished utilizing Zn amalgam in a hydrothermal reaction. All reactions were carried with no regard to O_2 exclusion, and the products are air stable.

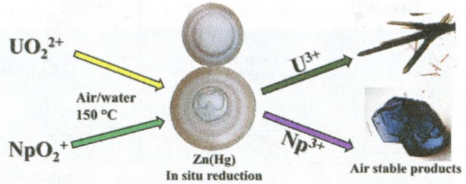

7467 S dx.doi.org/10.1021/ic500807y

Iron and Chromium Complexes Containing Tridentate Chelates Based on Nacnac and Imino- and Methyl-Pyridine Components: Triggering C—X Bond Formation

Wesley D. Morris, Peter T. Wolczanski,* Jörg Sutter, Karsten Meyer, Thomas R. Cundari, and Emil B. Lobkovsky

Base-induced 1,3-dehydroamination and complementary oxidation reactions generate unsaturation in a tridentate iminopyridine—nacnac ligand, leading to carbon—carbon and carbon—nitrogen bond formation reactions, some via radical character derived from redox noninnocence.

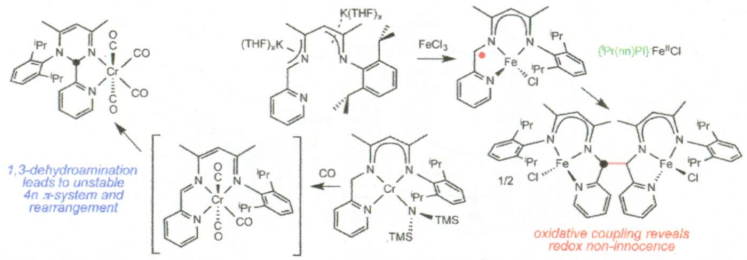

7485 S dx.doi.org/10.1021/ic500808q

Molecular and Electronic Structure of Cyclic Trinuclear Gold(I) Carbeniate Complexes: Insights for Structure/Luminescence/Conductivity Relationships

Roy N. McDougald Jr., Bhaskar Chilukuri, Huiping Jia, Michael R. Perez, Hassan Rabaâ, Xiaoping Wang, Vladimir N. Nesterov, Thomas R. Cundari,* Bruce E. Gnade,* and Mohammad A. Omary*

An experimental/computational study correlating solid-state structures and optical/electronic properties of $[Au_3(RN{=}COR')_3]$ cyclotrimers (R, R′ = H, Me, ^{n}Bu, or ^{t}Pe) is reported. Their solid-state photoluminescence spectra display a remarkable dependence on solid-state packing. Hole transport for $[Au_3(RN{=}COR')_3]$—doped in poly(9-vinylcarbazole)—produced a colossal 3-order-of-magnitide increase in current density, while single needles acted as molecular wires (p-type field effect transistor). Changes in R and R′ lead to distinctive variations in solid-state stacking, luminescence spectra, and conductive properties.

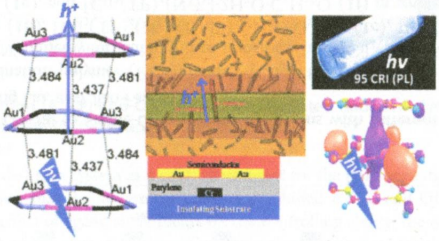

7500 Ⓢ dx.doi.org/10.1021/ic500829p

The Mechanism of Homogeneous CO_2 Reduction by Ni(cyclam): Product Selectivity, Concerted Proton–Electron Transfer and C–O Bond Cleavage

Jinshuai Song, Eric L. Klein, Frank Neese, and Shengfa Ye*

A computational study of the reaction mechanism of homogeneous CO_2 reduction catalyzed by Ni(cyclam) is detailed herein. The reaction yields CO only, and this product selectivity stems from the different stability of the Ni–CO_2 adducts (η^1-CO_2 vs η^1-OCO). Our calculations show that the reaction following the formation of the Ni–CO_2 complex is likely to proceed via concerted proton–electron transfer and C–O bond cleavage.

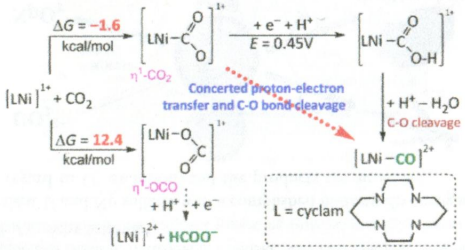

7508 Ⓢ dx.doi.org/10.1021/ic5008044

New Families of Hetero-tri-spin 2p–3d–4f Complexes: Synthesis, Crystal Structures, and Magnetic Properties

Lívia B. L. Escobar, Guilherme P. Guedes, Stéphane Soriano, Nivaldo L. Speziali, Alessandro K. Jordão, Anna Claudia Cunha, Vitor F. Ferreira, Catalin Maxim, Miguel A. Novak, Marius Andruh,* Maria G. F. Vaz,* and

Two families of heterospin 2p–3d–4f compounds with molecular formula $[Cu_3Ln_2(hfac)_8(OH)_4(N_3tempo)]$ (Ln = Gd, Tb, Dy) and $[CuLn_2(hfac)_8(N_3tempo)_2(H_2O)_2]$ (Ln = Gd, Dy) were obtained by a one pot reaction depending on the stoichiometric ratio used between the building blocks. The magnetic properties of all compounds were investigated by dc and ac measurements. The ac magnetic susceptibility measurements of Tb^{III} and Dy^{III} containing compounds revealed slow relaxation of the magnetization with magnetic quantum tunneling in zero field.

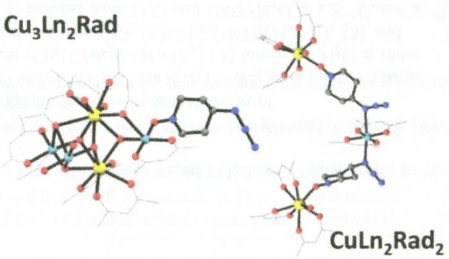

7518 dx.doi.org/10.1021/ic5008439

Prodigiosin Analogue Designed for Metal Coordination: Stable Zinc and Copper Pyrrolyldipyrrins

Tsuhen M. Chang, Sanhita Sinharay, Andrei V. Astashkin, and Elisa Tomat*

The pyrrolyldipyrrin motif, which characterizes the prodigiosin natural products of bacterial origin, is engineered to afford a stable tripyrrolic scaffold for coordination of transition metals. Prompt binding of zinc and copper ions occurs in the absence of added bases at room temperature. Full structural and spectroscopic characterization by X-ray diffraction and EPR/ENDOR techniques documents the hitherto elusive coordination of the Cu(II) ion in this ligand framework.

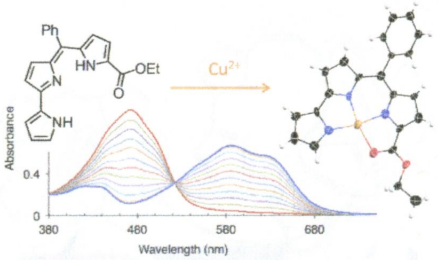

7527 dx.doi.org/10.1021/ic5008457

Series of Solvent-Induced Single-Crystal to Single-Crystal Transformations with Different Sizes of Solvent Molecules

Yuan-Chun He, Jin Yang,* Ying-Ying Liu, and Jian-Fang Ma*

A highly stable soft porous coordination polymer (PCP), namely $[Cu_3(TP)_4(N_3)_2(DMF)_2]\cdot 2H_2O\cdot 2DMF$ (**1**) (TP = 4-tetrazole pyridine and DMF = *N*,*N*′-dimethylformamide), can transform into $[Cu_3(TP)_4(N_3)_2(DMF)_2]\cdot 3C_6H_{12}$ (**1a**), $[Cu_3(TP)_4(N_3)_2(DMF)_2]\cdot 2C_5H_{10}$ (**1b**), $[Cu_3(TP)_4(N_3)_2(DMF)_2]\cdot H_2O\cdot C_{10}H_{18}$ (**1c**), $[Cu_3(TP)_4(N_3)_2(DMF)_2]\cdot C_4H_8O_2$ (**1d**), $[Cu_3(TP)_4(N_3)_2]\cdot 3C_4H_8O_2$ (**1e**), and $[Cu_3(TP)_4(N_3)_2]\cdot 2H_2O\cdot C_5H_{10}O$ (**1f**) in single-crystal to single-crystal (SCSC) manners upon exposure to different solvents, and shows guest selectivity for cyclopentane, cyclohexane, and decahydronaphthalene in SCSC fashions.

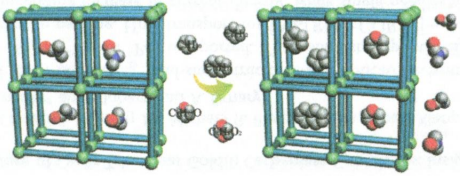

7534 S dx.doi.org/10.1021/ic500832u

Solvent Dependent Assembly of Lanthanide Metallacrowns Using Building Blocks with Incompatible Symmetry Preferences
Joseph Jankolovits, Jeff. W. Kampf, and Vincent L. Pecoraro*

Using geometric principles of coordination driven assembly, 8 lanthanide metallacrowns are shown to selectively assemble from Zn(II), Ln(III), and picoline hydroxamic acid through an intricate solvent dependence that is controlled by differential coordination of solvent molecules. The structural promiscuity is attributed to the symmetry incompatible building blocks, which are only capable of assembling macrocycles possessing geometrically strained dative bonds.

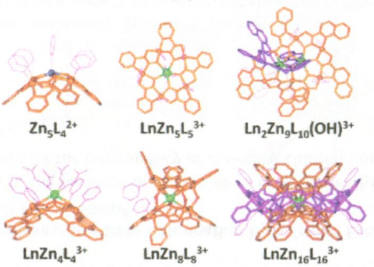

7547 S dx.doi.org/10.1021/ic500857b

Synthesis of Functional Phosphates $[P(C_2F_5)_3F_2X]^-$ from the Phosphorane Adduct $[P(C_2F_5)_3F_2(dmap)]$
Julia Bader, Nikolai Ignat'ev, and Berthold Hoge*

To develop the chemistry of weakly coordinating anions derived from $[P(C_2F_5)_3F_3]^-$, which is ideally suited for an application as ionic liquid, functional substituents X were attached to the phosphorane moiety $(C_2F_5)_3PF_2$. The reaction of the Lewis acid $(C_2F_5)_3PF_2$ with 4-(dimethylamino)pyridine (DMAP) quantitatively afforded the adduct $[P(C_2F_5)_3F_2(dmap)]$. The treatment with Brønsted acids HX yielded the corresponding phosphate anions $[P(C_2F_5)_3F_2X]^-$.

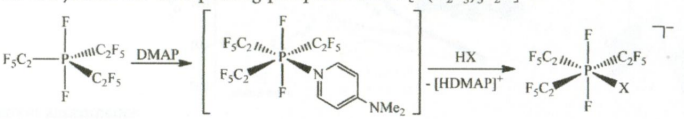

7554 S dx.doi.org/10.1021/ic500875m

Structures and Magnetic Properties of Two Analogous Dy_6 Wheels with Electron-Donation and -Withdrawal Effects
Biplab Joarder, Soumya Mukherjee, Shufang Xue, Jinkui Tang,* and Sujit K. Ghosh*

Two new analogous hexanuclear symmetric dysprosium wheels were isolated employing a mixed-ligand strategy. The structural differences induced by the introduction of divergent-natured auxiliary groups with distinct steric effect and electrostatic actions influence the orbital overlaps existent between the metal centers and ligands, as well as the local tensor of anisotropy on each dysprosium site and their relative orientations, consequently leading to incongruent magnetic behaviors.

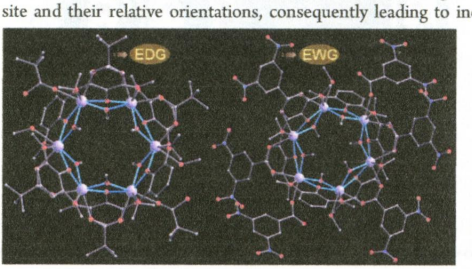

7561 S dx.doi.org/10.1021/ic500878w

Mediator Enhanced Water Oxidation Using $Rb_4[Ru^{II}(bpy)_3]_5[\{Ru^{III}_4O_4(OH)_2(H_2O)_4\}(\gamma\text{-}SiW_{10}O_{36})_2]$ Film Modified Electrodes

Si-Xuan Guo, Chong-Yong Lee, Jie Zhang,* Alan M. Bond,* Yurii V. Geletii, and Craig L. Hill*

Mediated electron transfer, an approach frequently used in the development of enzyme electrodes to facilitate the electron transfer between the enzyme and the electrode, has been successfully applied in the electrocatalytic oxidation of water with enhanced activity using solid state $Rb_4[Ru^{II}(bpy)_3]_5[\{Ru^{III}_4O_4(OH)_2(H_2O)_4\}(\gamma\text{-}SiW_{10}O_{36})_2]$.

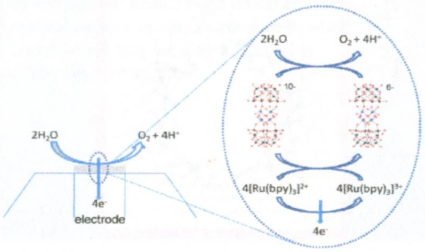

7571 S dx.doi.org/10.1021/ic500890r

Structure and Emissive Properties of Heterobimetallic Ln–Au Coordination Polymers: Role of Tb and Eu in Non-aurophilic $[^nBu_4N]_2[Ln(NO_3)_4Au(CN)_2]$ versus Aurophilic $Ln[Au(CN)_2]_3{\cdot}3H_2O/3D_2O$ Chains

John C. Ahern, Ryan J. Roberts, Philip Follansbee, Jeffrey McLaughlin, Daniel B. Leznoff, and Howard H. Patterson*

Luminescence and crystallographic studies have been carried out on five different dicyanoaurate(I) polymer chain frameworks, containing and lacking aurophilic interactions. In aurophilic frameworks interactions between gold(I) centers on neighboring chains facilitates energy transfer between Au and Ln as well as between two lanthanide ions. Such energy transfer is not observed in non-aurophilic frameworks, which have $^nBu_4N$ cations that keep the Au-containing chains from interacting.

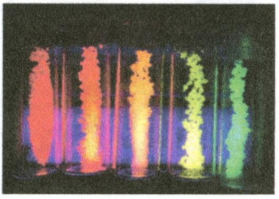

7580 S dx.doi.org/10.1021/ic5009347

Atom Transfer Radical Polymerization (ATRP) and Organometallic Mediated Radical Polymerization (OMRP) of Styrene Mediated by Diaminobis(phenolato)iron(II) Complexes: A DFT Study

Rinaldo Poli* and Michael P. Shaver

The action of a diaminobis(phenolato) iron system as a controlling agent for the polymerization of styrene has been addressed by a DFT study, supporting the view that the system operates by combined ATRP and OMRP moderating equilibria. The study also addresses the electronic effect of ligand substituents on the controlling ability, the effect of pressure on rates through volume calculations, and the effect of the spin state change on the activation barriers for the trapping processes.

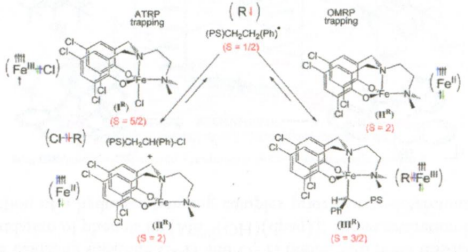

7591 S dx.doi.org/10.1021/ic500900n

Construction of Non-Interpenetrated Charged Metal–Organic Frameworks with Doubly Pillared Layers: Pore Modification and Selective Gas Adsorption

Susan Sen, Subhadip Neogi, Arshad Aijaz, Qiang Xu,* and Parimal K. Bharadwaj*

Variation of the pillar linker modulates the pore in a series of charged bipillar-layer frameworks. The selectivity of CO_2 gas adsorption over N_2 and CH_4 goes parallel with the pore size in these charged frameworks.

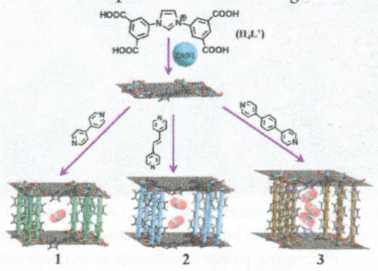

7599 S dx.doi.org/10.1021/ic500908r

Network Flexibility: Control of Gate Opening in an Isostructural Series of Ag-MOFs by Linker Substitution

Marcel Handke, Hanna Weber, Marcus Lange, Jens Möllmer, Jörg Lincke, Roger Gläser, Reiner Staudt, and Harald Krautscheid*

A series of 15 microporous silver MOFs with **lvt** topology and 2-fold network interpenetration is reported. Sorption studies and XRD patterns demonstrate the structural flexibility of the new materials, resulting in isotherms with one or two hysteresis loops. Pore diameters and pore volumes, gate-opening behavior, and the shape of hysteresis can be adjusted by the size and position of the linker substituents.

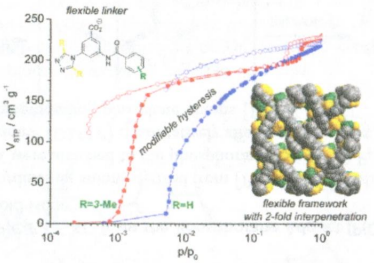

7608 S dx.doi.org/10.1021/ic5009413

Photoreduction of Pt(IV) Chloro Complexes: Substrate Chlorination by a Triplet Excited State

Tharushi A. Perera, Mehdi Masjedi, and Paul R. Sharp*

Photolysis of *trans*-$Pt(PEt_3)_2(R)(Cl)_3$ in the presence of alkenes gives *trans*-$Pt(PEt_3)_2(R)Cl$ and chlorinated alkenes, but no evidence for the intermediacy of molecular chlorine could be found.

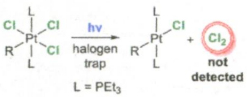

7622 dx.doi.org/10.1021/ic500943k

Saturation Kinetics in Phenolic O–H Bond Oxidation by a Mononuclear Mn(III)–OH Complex Derived from Dioxygen

Gayan B. Wijeratne, Briana Corzine, Victor W. Day, and Timothy A. Jackson*

The $[Mn^{III}(OH)(dpaq)]^+$ complex is formed by oxygenation of the corresponding $[Mn^{II}(dpaq)](OTf)$ compound and represents a relatively rare example of a structurally characterized mononuclear hydroxomanganese(III) complex. $[Mn^{III}(OH)(dpaq)]^+$ capable of oxidizing substrate C–H and O–H bonds with bond dissociation free energies of up to 78.5 kcal/mol in acetonitrile. The oxidation of phenols by $[Mn^{III}(OH)(dpaq)]^+$ shows saturation behavior, which is interpreting in terms of the equilibrium formation of a hydrogen-bonding complex prior to rate-determining concerted proton–electron transfer.

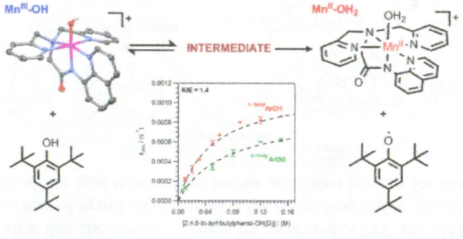

7635 dx.doi.org/10.1021/ic5009363

Enhancement of Optical Faraday Effect of Nonanuclear Tb(III) Complexes

Takayuki Nakanishi,* Yuki Suzuki, Yoshihiro Doi, Tomohiro Seki, Hitoshi Koizumi, Koji Fushimi, Koji Fujita, Yukio Hinatsu, Hajime Ito, Katsuhisa Tanaka, and Yasuchika Hasegawa*

This study presents a novel sandglass-shaped nonanuclear Tb(III) complex, which induces the Faraday effect, making it of practical interest to researchers due to its remarkable magneto–optical properties. The effective Faraday rotation in nonanuclear Tb(III) complexes was observed in the visible region (400–700 nm). The Faraday rotation efficiency of nonanuclear Tb(III) complexes is 150 times greater than that of commercial Tb(III) oxide glasses for optical isolators.

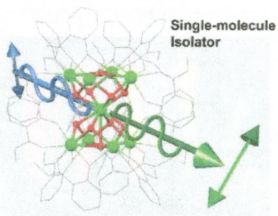

7642 dx.doi.org/10.1021/ic500957y

A Chiral, Low-Cytotoxic $[Ni_{15}]$-Wheel Complex

Simon Muche, Irina Levacheva, Olga Samsonova, Linh Pham, George Christou, Udo Bakowsky, and Małgorzata Hołyńska*

Synthesis and the properties relevant for biology/materials science of a chiral, rare, odd-membered wheel-like topology $[Ni_{15}]$ complex with a Schiff-base ligand are described.

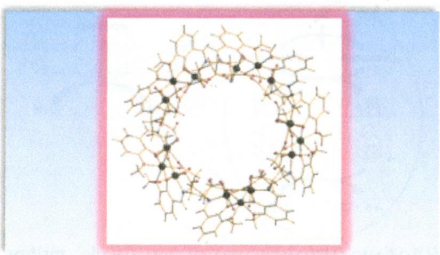

7650 dx.doi.org/10.1021/ic500965v

Highly Distorted Uranyl Ion Coordination and One/Two-Dimensional Structural Relationship in the $Ba_2[UO_2(TO_4)_2]$ (T = P, As) System: An Experimental and Computational Study

Shijun Wu, Piotr M. Kowalski, Na Yu, Thomas Malcherek, Wulf Depmeier, Dirk Bosbach, Shuao Wang, Evgeny V. Suleimanov, Thomas E. Albrecht-Schmitt,* and Evgeny V. Alekseev*

Three new uranium compounds with $Ba_2[UO_2(TO_4)_2]$ (T = P, As) compositions were synthesized. There are two polymorphic modifications observed in phosphate system. α-$Ba_2[UO_2(PO_4)_2]$ and β-$Ba_2[UO_2(PO_4)_2]$ are topologically identical, but α-phase is heavily distorted with respect to β-phase. Experimental evidence as well as density functional theory (DFT) calculations suggest that α-phase surprisingly is more stable than β-phase.

7661 dx.doi.org/10.1021/ic5009686

Crystal Structure and Magnetic Properties of the $S = {}^1/_2$ Quantum Spin System $Cu_7(TeO_3)_6F_2$ with Mixed Dimensionality

Shichao Hu, Amber Mace, Mats Johnsson,* Vladimir Gnezdilov, Peter Lemmens, Joshua Tapp, and Angela Möller

The new oxofluoride $Cu_7(TeO_3)_6F_2$ crystallizes in the space group $P\bar{1}$. The crystal structure constitutes a Cu−O framework with channels where the terminating F^- ions and the stereochemically active lone-pairs on Te^{4+} are located. Magnetic susceptibility, specific heat, and Raman scattering measurements provide evidence for that the magnetic degrees of freedom of the Cu−O−Cu segments lead to a mixed dimensionality.

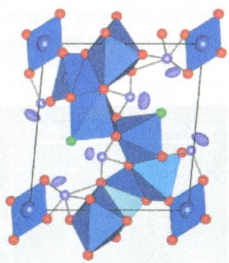

7668 dx.doi.org/10.1021/ic500963q

A Single-Component White-Emitting $CaSr_2Al_2O_6:Ce^{3+}$, Li^+, Mn^{2+} Phosphor via Energy Transfer

Yanyan Li, Yurong Shi, Ge Zhu, Quansheng Wu, Hao Li, Xicheng Wang, Qian Wang, and Yuhua Wang*

A series of single-component $CaSr_2Al_2O_6:Ce^{3+}$, Li^+, Mn^{2+} phosphors were synthesized by the high-temperature solid-state reaction. The crystallographic cation sites occupancy, luminescence properties, and the energy transfer mechanism from the Ce^{3+} to Mn^{2+} ions of $CaSr_2Al2O_6:Ce^{3+}$, Li^+, Mn^{2+} phosphors were investigated by means of photoluminescence and decay curves in detail. Under ultraviolet excitation, tunable colors including warm-white emission can be obtained by adjusting the ratio of Ce^{3+} and Mn^{2+} ions in $CaSr_2Al_2O_6$.

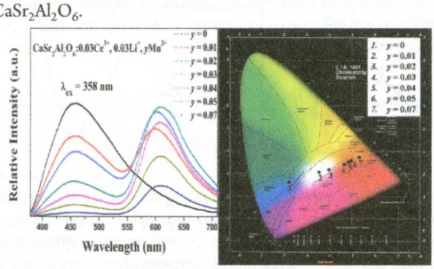

7676 S

dx.doi.org/10.1021/ic500986x

Spectral and Electronic Properties of Nitrosylcobalamin

Ivan G. Pallares and Thomas C. Brunold*

Various spectroscopic and computational techniques were used to generate experimentally validated electronic structure descriptions for the "base-on" and "base-off" forms of nitrosylcobalamin. The principal Co−ligand bonding interactions were examined further by carrying out natural bond orbital analyses. Our results indicate that the Co $3d_{z^2}$ orbital engages in a highly covalent bonding interaction with one of the NO π^* orbitals and that the Co−NO bond is strengthened further by sizable π-backbonding interactions.

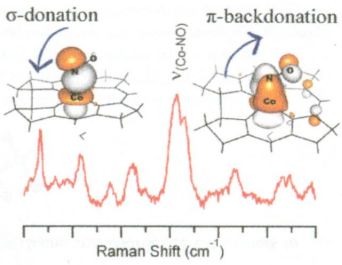

7692 S

dx.doi.org/10.1021/ic5009895

Three N−H Functionalized Metal−Organic Frameworks with Selective CO_2 Uptake, Dye Capture, and Catalysis

Yu Zhu, Yan-Mei Wang, Sheng-Yun Zhao, Pan Liu, Chao Wei, Yun-Long Wu, Chang-Kun Xia, and Ji-Min Xie*

An N−H functionalized ligand was synthesized, and we have obtained three different network topologies with empty spaces by changing the metal cations. The N−H groups on pyrazine can enhance CO_2 adsorptions. Cu-DDQ shows high selectivity for CO_2/N_2 due to the small adsorption of N_2. Zn-DDQ and Cu-DDQ with different shapes of pores are promising materials for fast separation of MB/other and CV/other mixtures, respectively. The cyanosilylation reactions indicate that Cu-DDQ has greater Lewis acidity.

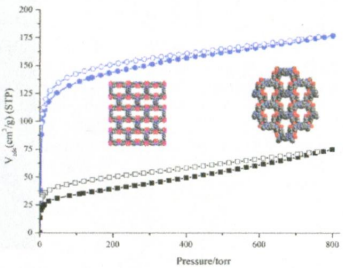

7700 S

dx.doi.org/10.1021/ic500991x

Understanding Lanthanoid(III) Hydration Structure and Kinetics by Insights from Energies and Wave functions

Jun Zhang,* Norah Heinz, and Michael Dolg*

The hydration of all trivalent lanthanoid (Ln) ions is studied theoretically from two aspects: energy and wave function. We suggest that the capping Ln−O bonds of moderate strength, which occur for intermediate lanthanoids, are advantageous for the formation of a bicapped trigonal prism intermediate during water exchange. The "shorter and weaker" behavior of capping Ln−O bonds is believed to determine the hydration behavior of lanthanoid(III) ions.

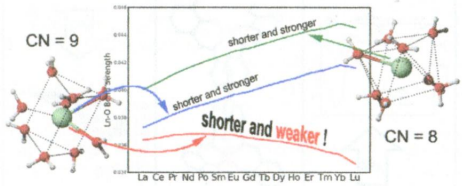

7709 Ⓢ dx.doi.org/10.1021/ic500999k

Iridium(III) Complexes with Phenyl-tetrazoles as Cyclometalating Ligands

Filippo Monti, Andrea Baschieri, Isacco Gualandi, Juan J. Serrano-Pérez, José M. Junquera-Hernández, Domenica Tonelli, Andrea Mazzanti, Sara Muzzioli, Stefano Stagni, Cristina Roldan-Carmona, Antonio Pertegás, Henk J. Bolink, Enrique Ortí,* Letizia Sambri,* and Nicola Armaroli*

A novel two-step synthetic strategy, based on a silver-assisted cyclometalation reaction with $IrCl_3$, allows the preparation of the first cationic Ir(III) complexes with tetrazole units on the C^^N cyclometallating ligand. Three of them exhibit high PLQY in solution and in the solid state (55−70%) and the highest-energy MLCT/LLCT emission bands ever reported among cationic iridium complexes without fluorine residues on the cyclometalated ligands. A comprehensive study, from theoretical calculations to LEC devices, is presented.

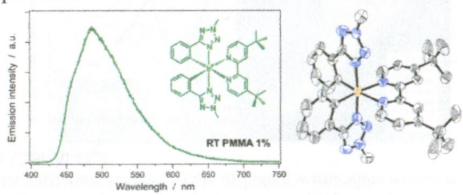

7722 Ⓢ dx.doi.org/10.1021/ic5010243

Nanostructures in Te/Sb/Ge/Ag (TAGS) Thermoelectric Materials Induced by Phase Transitions Associated with Vacancy Ordering

Thorsten Schröder, Tobias Rosenthal, Nadja Giesbrecht, Markus Nentwig, Stefan Maier, Heng Wang, G. Jeffrey Snyder, and Oliver Oeckler*

Adjusting the Ag/Sb ratio in TAGS thermoelectric materials leads to cation vacancies. These have different ordering possibilities which involve a significantly extended structural chemistry as compared to conventional TAGS materials and can be utilized to induce nanostructures in the material. The vacancies scatter phonons efficiently which means a low phononic contribution to the thermal conductivity and increases the ZT value for this TAGS material below 200 °C.

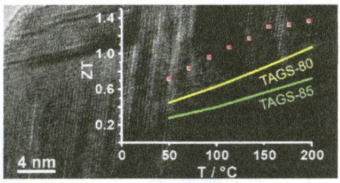

7730 Ⓢ dx.doi.org/10.1021/ic501054z

Small Molecule Activation Chemistry of Cu−Fe Heterobimetallic Complexes Toward CS_2 and N_2O

Upul Jayarathne, Sean R. Parmelee, and Neal P. Mankad*

Activation of CS_2 and N_2O was observed with Cu−Fe heterobimetallic complexes, including stoichiometric O atom transfer from N_2O.

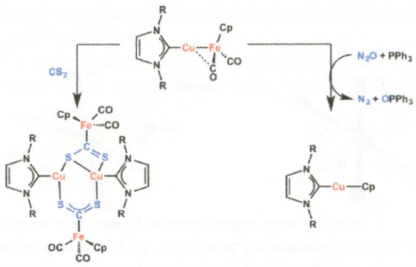

7738 dx.doi.org/10.1021/ic501051q

Magnetic and Luminescent Binuclear Double-Stranded Helicates

Paula Cucos, Floriana Tuna,* Lorenzo Sorace,* Iulia Matei, Catalin Maxim, Sergiu Shova, Ruxandra Gheorghe, Andrea Caneschi, Mihaela Hillebrand, and Marius Andruh*

The helicand resulting from the 2:1 condensation reaction between *o*-vanillin and 4,4′-diaminodiphenyl ether provides three new double-stranded helicates containing Co(II), Cu(II), and, respectively, Zn(II) ions. For the cobalt derivative, the dynamic susceptibility measurements indicate that each metal ion shows slow relaxation of the magnetization in an applied dc field. The zinc helicate shows luminescence in solution.

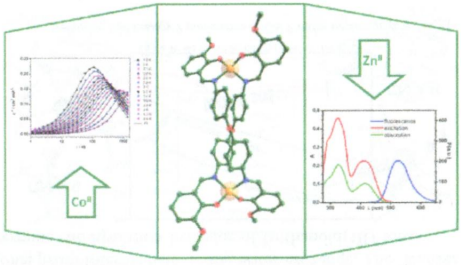

7748 dx.doi.org/10.1021/ic501063j

A Double Substitution of Mg^{2+}–Si^{4+}/Ge^{4+} for $Al_{(1)}^{3+}$–$Al_{(2)}^{3+}$ in Ce^{3+}-Doped Garnet Phosphor for White LEDs

Mengmeng Shang, Jian Fan, Hongzhou Lian, Yang Zhang, Dongling Geng, and Jun Lin*

The Mg^{2+}–Si^{4+}/Ge^{4+} incorporation of Mg^{2+}–Si^{4+}/Ge^{4+} into Ce^{3+}-doped $Y_3Al_5O_{12}$ garnet phosphors leads to an obvious red shift of usual Ce^{3+} yellow emission and produces an additional site for Ce^{3+} occupation to give blue-green emission with ultraviolet excitation.

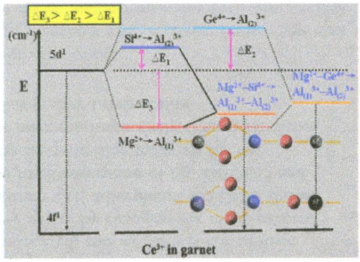

7756 dx.doi.org/10.1021/ic5011264

Quaternary Arsenides $ACdGeAs_2$ (A = K, Rb) Built of Ethane-Like Ge_2As_6 Units

Mansura Khatun, Stanislav S. Stoyko, and Arthur Mar*

Ge_2As_6 polyanions, which resemble ethane in staggered conformation, form linear chains and coordinate Cd centers in quaternary arsenides $ACdGeAs_2$ (A = K, Rb).

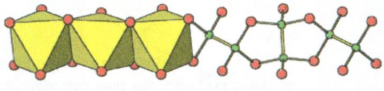

7763 S dx.doi.org/10.1021/ic501133n

Mono-, Di-, and Triborylphosphine Analogues of Triarylphosphines

Jonathan A. Bailey, Marten Ploeger, and Paul G. Pringle*

Tris(diazaborinyl)phosphine has steric properties comparable to those of PPh_3 and electronic properties comparable to those of PMe_3.

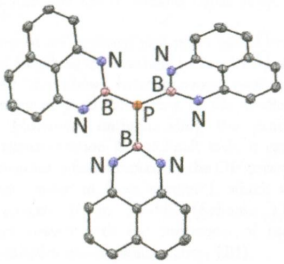

7770 S dx.doi.org/10.1021/ic501141m

Copper(II)-Catalyzed Disulfide Scission—Stepwise Aerobic Oxidative Cleavage to Sulfinate and Sulfonate and Reductive Anaerobic Cleavage to Thiols

Isha Lumb, Maninder Singh Hundal,* and Geeta Hundal*

Cu(II)-catalyzed oxidative and reductive cleavage of a disulfide bond in a disulfidedipicolinamide, **L**, is reported for the first time. Cu(II) gives a complete oxidation up to sulfonates, forming a thermally stable 2D complex, while Ag(I) oxidizes it up to sulfinate only. The reductive cleavage of S−S bond yields to thiols, which undergo *in situ* formation of a new C−S bond, resulting in a tetranuclear complex of Cu(II) with deprotonated amide groups.

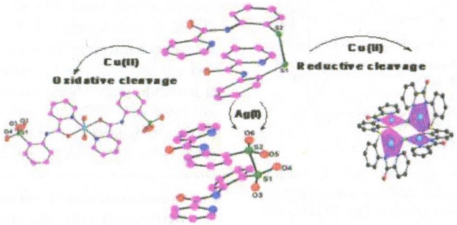

7780 S dx.doi.org/10.1021/ic5013457

High-Valent Chromium−Oxo Complex Acting as an Efficient Catalyst Precursor for Selective Two-Electron Reduction of Dioxygen by a Ferrocene Derivative

Shuo Liu, Kentaro Mase, Curt Bougher, Scott D. Hicks, Mahdi M. Abu-Omar,* and Shunichi Fukuzumi*

Efficient catalytic two-electron reduction of dioxygen by octamethylferrocene produced hydrogen peroxide using a high-valent chromium(V)−oxo corrole complex, $[(tpfc)Cr^{V}(O)]$, as a catalyst precursor in the presence of trifluoroacetic acid in acetonitrile via inner-sphere electron transfer from $[(tpfc)Cr^{III}(OH_2)]$ to dioxygen as the rate-determining step in the catalytic cycle.

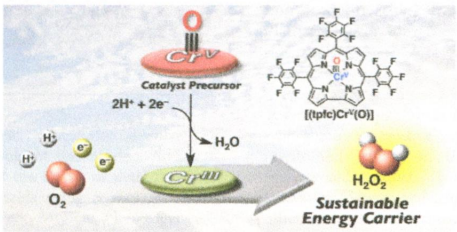

7789 (S) dx.doi.org/10.1021/ic5015048

Impact of d-Orbital Occupation on Metal–Carbon Bond Functionalization

E. Chauncey Garrett III, Travis M. Figg, and Thomas R. Cundari*

A series of first-row transition metal–methyl complexes was modeled for two pathways: an organometallic Baeyer–Villiger (OMBV) and a two-step, redox oxy-insertion. The OMBV mechanism is only preferred when the metal–methyl's d^n count renders a chemically infeasible formal oxidation state for an oxo-methyl intermediate. Destabilization of the oxo-Me intermediate in the redox pathway effectively removes one thermodynamic "sink." Future experiments should focus on oxy-insertion with weaker oxidants and establishing both thermodynamic and kinetic oxygen-atom transfer potentials.

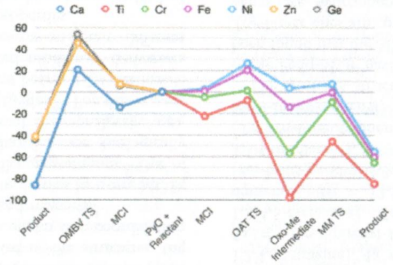

(S) Supporting Information available via online article